

theory and fundamental aspects

Theory of photon interference X-ray absorption fine structure

Yoshinori Nishino^{a*} and Gerhard Materlik^b

^a*Japan Synchrotron Radiation Research Institute JASRI, 1-1-1 Kouto, Mikazuki-cho, Sayo-gun, Hyogo 679-5198, Japan, and ^bHamburger Synchrotronstrahlungslabor HASYLAB at Deutsches Elektronen-Synchrotron DESY, Notkestrasse 85, D-22607 Hamburg, Germany. E-mail: nishino@spring8.or.jp*

The theory of photon interference x-ray absorption fine structure (π XAFS) is described. Due to coherent x-ray scattering from atoms, a spatial variation of the x-ray intensity is produced inside the sample. The intensity at the x-ray absorbing atom changes according to the incident energy. Thus π XAFS in extended absorption spectra is produced. It extends in a wide energy range over absorption edges. For powders the π XAFS formula has equivalent form as the EXAFS formula, and the Fourier transform provides distances of neighboring atoms from the absorbing atom. Due to a long mean free path of the photon, π XAFS for powders contains sharp structures. They are explained as a crystal grain orientation averaging of the x-ray standing wave effect.

Keywords: π XAFS; theory.

In photoabsorption through the photoionization process, the incident photon is absorbed by a core-level electron, and produces a pair of photoelectron and core-hole. Both the initial-state photon and the final-state photoelectron may be coherently scattered from surrounding atoms of the absorbing atom. The initial state of photoionization process is therefore the photon interference state, and the final state is the photoelectron interference state. The photoelectron interference in the final state changes with the incident energy, and it causes extended x-ray absorption fine structure (EXAFS) in x-ray absorption spectra.

In a similar way, the photon interference in the initial state varies with the incident energy or angle, and accordingly the x-ray intensity at the absorbing atom position changes. The change is observed in x-ray absorption measurements. The effect is especially strong near the Bragg condition, because a strong x-ray standing wave (XSW) is formed inside the sample (Batterman & Cole, 1964; Ohta, 1985). X-ray absorption for a pure single crystal near the Bragg condition is nowadays widely used for determination of the absorbing atom position relative to the diffraction plane (Bedzyk & Materlik, 1985; Zegenhagen, 1993).

The photon interference effect in x-ray absorption is also used in multiple-energy x-ray holography (MEXH) (Gog *et al.*, 1996). In the MEXH method, the x-ray absorption is measured in a wide (ideally full 4π) angular and energy ranges. The modulation of absorption in reciprocal space is considered to be a hologram (Nishino & Materlik, 1999). It is converted to three-dimensional image of neighboring atoms in real space by a method like Fourier transformation. It is clear from the success of MEXH that only one neighboring atom can produce an observable photon interference effect on x-ray absorption.

The two effects in x-ray absorption, the final-state photoelectron and initial-state photon interference effects, are consistently

treated in the quantum theory by Nishino & Materlik (1999). It was shown that in x-ray absorption spectra, in addition to EXAFS due to the photoelectron interference effect, there is a structure due to the photon interference effect from neighboring atoms. The new structure is named photon interference x-ray absorption fine structure (π XAFS) (Nishino *et al.*, 2000). π XAFS remains also in a sample without preferred orientation as powders (Nishino *et al.*, 2000). π XAFS for powders is also important in a practical application, because its Fourier transformation gives radial positions of the neighboring atoms as in the case of EXAFS. In this paper we show the theoretical formulation of π XAFS.

The linear absorption coefficient due to the photoionization is proportional to the total photoionization cross section. The total photoionization cross section σ_{PI} for the non-relativistic photoelectron is defined in terms of the transition matrix T_{fi} as

$$\sigma_{\text{PI}} = \frac{(2\pi)^4 m_e k_e}{\hbar^3 c} \int d\Omega_{\hat{k}_e} |T_{fi}|^2, \quad (1)$$

where $\mathbf{k}_e = k_e \hat{\mathbf{k}}_e$, m_e and $\Omega_{\hat{k}_e}$ are the wave number vector, mass and solid angle of photoelectron, respectively. We consider three contributions shown in fig. 1 to the transition matrix T_{fi} . They are (a) the atomic contribution, (b) the initial-state photon interaction contribution and (c) the final-state photoelectron interaction contribution. For a sample with a preferred orientation of neighboring atoms, it is given by

$$T_{fi} = C(E_x) \times \left[\epsilon \cdot \hat{\mathbf{k}}_e - r_e \sum_{i \neq 0} (\epsilon \cdot \hat{\mathbf{k}}_e - \epsilon \cdot \hat{\mathbf{r}}_i \hat{\mathbf{k}}_e \cdot \hat{\mathbf{r}}_i) \frac{f_i^x(|\mathbf{k}_x + \mathbf{k}_x \hat{\mathbf{r}}_i|)}{r_i} e^{i(k_x r_i + \mathbf{k}_x \cdot \mathbf{r}_i)} + \sum_{i \neq 0} \epsilon \cdot \hat{\mathbf{r}}_i \frac{f_i^e(|\mathbf{k}_e - \mathbf{k}_e \hat{\mathbf{r}}_i|)}{r_i} e^{i(k_e r_i - \mathbf{k}_e \cdot \mathbf{r}_i)} \right], \quad (2)$$

in the single-scattering plane wave approximation (Nishino & Materlik, 1999). The approximation is appropriate for, e.g., a small single crystal. $C(E_x)$ in eq. (2) is a function of the incident photon energy E_x . r_e denotes the classical electron radius. f_i^x is the atomic form factor of photon scattering, f_i^e the scattering amplitude of electron scattering from the i th atom. The sums over i run over all neighboring atoms. Assuming that the second and third terms of eq.(2) are always smaller than the first term, one obtains

$$\sigma_{\text{PI}}(E_x, \hat{\mathbf{k}}_x, \epsilon) = \sigma_0(E_x) [1 + \chi^x(E_x, \hat{\mathbf{k}}_x, \epsilon) + \chi^e(E_x, \epsilon)], \quad (3)$$

by neglecting modulo-square of the second and third term of eq. (2). $\sigma_0(E_x)$ is the total photoionization cross section for an isolated atom. χ^x and χ^e are oscillating functions in energy due to the interference of photons and photoelectrons, respectively. The explicit expressions are given by

$$\begin{aligned} \chi^x(E_x, \hat{\mathbf{k}}_x, \epsilon) &= -2r_e \text{Re} \sum_{i \neq 0} [1 - (\epsilon \cdot \hat{\mathbf{r}}_i)^2] \\ &\times \frac{f_i^x(|\mathbf{k}_x + \mathbf{k}_x \hat{\mathbf{r}}_i|)}{r_i} e^{i(k_x r_i + \mathbf{k}_x \cdot \mathbf{r}_i)}, \end{aligned} \quad (4)$$

and

$$\chi^e(E_x, \epsilon) = -\frac{3}{k_e} \sum_{i \neq 0} \frac{(\epsilon \cdot \hat{\mathbf{r}}_i)^2}{r_i^2} \text{Im} [f_i^e(2k_e) e^{2ik_e r_i}]. \quad (5)$$

$2k_e$ in the argument of f_i^e denotes the backscattering geometry. The photon interference contribution χ^x of eq. (4) is a known formula

for MEXH (Nishino & Materlik, 1999; Adams *et al.*, 1998). The photoelectron interference contribution χ^e of eq. (5) is the single-scattering contribution to EXAFS. Although the photon interference effect χ^x is typically small, it gives a non-negligible contribution to x-ray absorption spectra at energies far from absorption edges. Similarly, the photoelectron interference contribution χ^e should be taken into account in MEXH analysis.

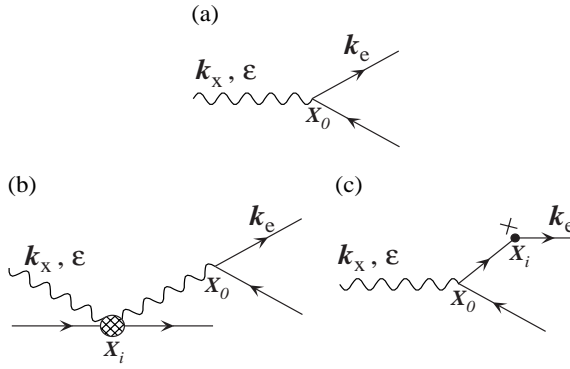


Figure 1

Feynman diagrams of photoionization process. Wavy lines are photons with wave number vector $\mathbf{k}_x = k_x \hat{\mathbf{k}}_x$ and polarization ϵ . Straight lines are electrons. Photoelectrons are shown with momentum \mathbf{k}_e . Electrons with arrows to the left are core-holes. (a) The atomic contribution. The incident photon scatters a core-level electron in the atom at X_0 and creates the photoelectron and core-hole. (b) The scattering of photon in the initial state. The photon is scattered by an electron of the i th neighboring atom at X_i ($r_i = r_i \hat{\mathbf{r}} = X_i - X_0$). The circle with hatch contains all photon-electron interaction diagrams. The Thomson scattering corresponding to the seagull diagram gives a dominant contribution. (c) The Coulomb scattering of photoelectron in the final state.

If the sample does not have preferred orientation of neighboring atoms, as powders, the total photoionization cross section needs to be averaged over the neighbor orientations $\hat{\mathbf{r}}_i$. The neighbor orientation random average $\bar{\chi}^e$ of the photoelectron interference contribution χ^e is simply given by eq. (5) with replacing the factor $(\epsilon \cdot \hat{\mathbf{r}}_i)^2$ by $1/3$,

$$\bar{\chi}^e(E_x) = -\frac{1}{k_e} \sum_{i \neq 0} \frac{1}{r_i^2} \text{Im} [f_i^e(2k_e) e^{2ik_e r_i}] . \quad (6)$$

The $\hat{\mathbf{r}}_i$ random average of χ^x is obtained with a similar calculation procedure as in the EXAFS case (Lee, 1976). By using the partial wave expansion,

$$f_i^x(|\mathbf{k}_x + k_x \mathbf{r}_i|) = \sum_{l=0}^{\infty} f_{i,l}^x P_l(\cos(\hat{\mathbf{k}}_x \cdot \hat{\mathbf{r}}_i)) , \quad (7)$$

$$e^{i\mathbf{k}_x \cdot \mathbf{r}_i} = \sum_{l=0}^{\infty} (2l+1)(i)^l j_l(kr_i) P_l(\cos(\hat{\mathbf{k}}_x \cdot \hat{\mathbf{r}}_i)) , \quad (8)$$

$$(\epsilon \cdot \hat{\mathbf{r}}_i)^2 = \frac{8\pi}{15} \sum_{m=-2}^2 Y_{2m}^*(\epsilon) Y_{2m}(\hat{\mathbf{r}}_i) + \frac{1}{3} , \quad (9)$$

and the orthogonal relation of Legendre functions,

$$\int_{-1}^1 dz P_l(z) P_{l'}(z) = \frac{2}{2l+1} \delta_{l,l'} , \quad (10)$$

one obtains

$$\begin{aligned} \bar{\chi}^x(E_x) &= -4\pi r_e \text{Re} \sum_{i \neq 0} \frac{e^{i k_x r_i}}{r_i} \\ &\times \left[\sum_l (i)^l f_l^x(k_x) \left(j_l(k_x r_i) - \left(\frac{\partial}{\partial (k_x r_i)} \right)^2 j_l(k_x r_i) \right) \right] \end{aligned} \quad (11)$$

Assuming that the inter-atomic distance is longer than $1/k_x$, we employ the asymptotic form of spherical Bessel functions j_l ,

$$j_l(k_x r_i) \rightarrow \frac{\cos(k_x r_i - \frac{n+1}{2}\pi)}{k_x r_i} \quad (k_x r_i \rightarrow \infty) , \quad (12)$$

and obtain

$$\bar{\chi}^x(E_x) = -\frac{r_e}{k_x} \sum_{i \neq 0} \frac{1}{r_i^2} \text{Im} [f_i^x(2k_x) e^{2ik_x r_i} - f_i^x(0)] . \quad (13)$$

$f_i^x(0)$ term is non-oscillating. The contribution of Thomson scattering to $f_i^x(0)$ term cancels exactly with the term arising from the modulo-square of the second term of eq. (2). The cancellation is proven by using the optical theorem

$$\begin{aligned} \text{Im} f_i^{\text{Thomson}}(0) &= \\ -\frac{r_e k_x}{4\pi} \int d\Omega \hat{\mathbf{k}}'_x &\left[1 - (\epsilon \cdot \hat{\mathbf{k}}'_x)^2 \right] |f_i^{\text{Thomson}}(|\mathbf{k}'_x - \mathbf{k}_x|)|^2 \end{aligned} \quad (14)$$

Eq. (14) is obtained by applying the general form of the optical theorem

$$\text{Im} T_{ii} = \pi \sum_f \delta(E_f - E_i) |T_{fi}|^2 \quad (15)$$

to the transition matrix of Thomson scattering

$$T^{\text{Thomson}} = -\hbar c r_e \frac{\epsilon \cdot \epsilon'}{(2\pi)^2 k_x} f_i^{\text{Thomson}}(|\mathbf{k}'_x - \mathbf{k}_x|) . \quad (16)$$

The final result for π XAFS (oscillation contribution) for a random orientation sample is thus given by

$$\bar{\chi}^x(E_x) = -\frac{r_e}{k_x} \sum_{i \neq 0} \frac{1}{r_i^2} \text{Im} [f_i^x(2k_x) e^{2ik_x r_i}] . \quad (17)$$

π XAFS $\bar{\chi}^x$ of eq. (17) and EXAFS $\bar{\chi}^e$ of eq. (6) are of equivalent form. It is important to note that the π XAFS oscillation $\bar{\chi}^x$ is periodic in the photon wavenumber k_x , whereas the EXAFS oscillation $\bar{\chi}^e$ is periodic in the photoelectron wavenumber k_e . Therefore the Fourier transform of π XAFS with respect to $2k_x$ gives peaks corresponding to distances of neighboring atoms from the absorbing atom. Information of short range order of the sample is thus obtained in the same manner as in the EXAFS case. The frequency of $\bar{\chi}^x$ depends on the distance. The slowest oscillation is obtained for the nearest neighbor distance (e.g. the energy periodicity of 2.4 keV for a typical bond length of 2.6 Å). Relative amplitude of π XAFS to EXAFS measured at identical k is $\bar{\chi}^x / \bar{\chi}^e = r_e f^x / f^e$. For example, for Pt the ratio is 1.0×10^{-3} at $k \approx 12 \text{ \AA}^{-1}$.

Fig. 2 shows a simulation of π XAFS for a platinum power obtained from the π XAFS formula eq. (17). The Debye-Waller factor $\exp(-2\sigma^2 k_x^2)$ and the attenuation factor $\exp(-2r_i/l_x(E_x))$ were also taken into consideration. Here σ^2 is the mean-square relative displacement of atoms, and $l_x(E_x)$ is the photon mean free path. For simplicity, correlated atomic motions were neglected in the estimation of σ^2 , and twice the value in x-ray diffraction was assumed. The cluster for the simulation had a radius of 150 Å.

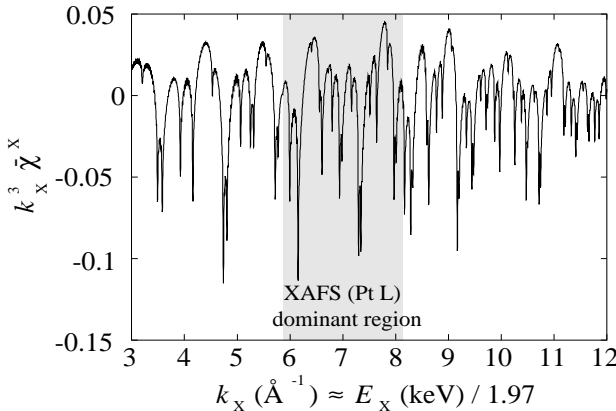


Figure 2

Simulation of π XAFS for a Pt powder. π XAFS extends in a wide energy range over absorption edges. Pt absorption edges are at 5.86 \AA^{-1} (L_{III}), 6.73 \AA^{-1} (L_{II}) and 7.03 \AA^{-1} (L_I). In the normalized absorption $(\mu - \mu_0)/\mu_0$ measured in experiments, there is an additional contribution of EXAFS. In the hatched region (within a few keV above absorption edges) the EXAFS signal is larger than the π XAFS signal. Here μ is the linear absorption coefficient, and μ_0 is its atomic contribution.

Although the formulae of EXAFS and π XAFS are of equivalent form, the π XAFS signal in fig. 2 looks differently from the EXAFS signal. The π XAFS signal contains sharp and negative structures. They are made up of many frequency modes: low frequencies from near coordination shells, and high frequencies from far coordination shells. On the other hand, the EXAFS signal is of low frequency. The difference stems from longer mean free path of photons than that of photoelectrons.

Information on long range order is also obtained from the π XAFS signal for powders. Because the characteristic sharp structure appears at the incident wavelength where the corresponding Bragg angle θ_B is $\pi/2$ (backward diffraction), the diffraction plane separation is determined. The origin of this structure is explained in fig. 3. The top plot of fig. 3 shows the Du Mond diagram, where the wavelength of a sharp structure position is denoted by $\lambda_{\pi/2}$. If the incident wavelength is equal or shorter than $\lambda_{\pi/2}$, powder diffraction occurs, and diffracted photons form the Debye-Scherrer cone with the half apex angle of $2\theta_B$. The bottom two plots of fig. 3 show the dependence of χ^x on the incident angle (the orientation of a crystal grain in powders). For powders χ^x should be averaged over the incident angle. If the incident angle for a crystal grain is close to the Bragg angle, a strong XSW field is formed inside the grain, and it produces a large dependence of absorption on the grain orientation. At the incident wavelength where the corresponding Bragg angle θ_B is not close to $\pi/2$, e.g. at the incident wavelength λ' in fig. 3, stronger (weaker) absorption than μ_0 is observed for grains with higher (lower) incident angle than θ_B (the bottom left plot of fig. 3). Thus contributions of grains with higher and lower incident angles than θ_B cancel to produce an averaged absorption. In difference to this case, if the incident wavelength is close to $\lambda_{\pi/2}$, the incident angles larger than θ_B and, consequently, lattice planes with higher absorption than μ_0 do not exist. Therefore only near $\lambda_{\pi/2}$ the XSW effect does not cancel by the grain orientation averaging. Moreover the Bragg reflection width is wide for $\theta_B = \pi/2$, (Kohra & Matsushita, 1972; Graeff & Materlik, 1982; Caticha & Caticha-Ellis, 1982), and it makes the π XAFS sharp structure large.

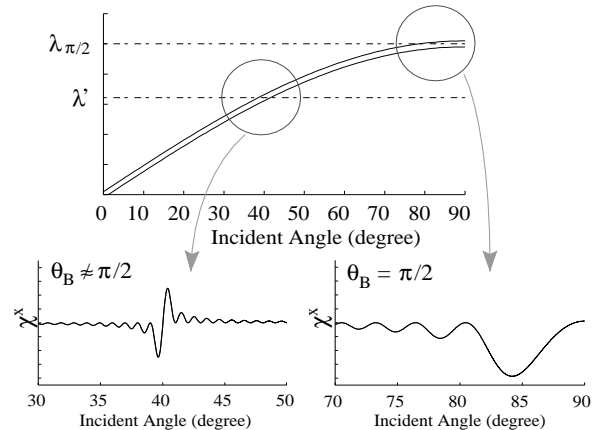


Figure 3

Explanation of sharp and negative structure in π XAFS for powders. The top plot is the Du Mond diagram. The bottom two plots show the dependence of χ^x on the incident angle. Two different incident wavelengths are considered. The bottom left is in the case that the Bragg angle is not close to $\pi/2$. The bottom right is in the case that it is $\pi/2$.

It should be noted that the total elastic scattering cross section of photons also exhibits a structure at $\lambda_{\pi/2}$. A positive step structure is expected, because the Bragg diffraction channel opens at this wavelength. In absorption measurements in transmission mode, both the true absorption (photoionization) and scattering contribute, therefore a careful treatment of scattering is necessary. The extinction effect will also be important in all detection modes of x-ray absorption, if the crystal grain size is large. In this case, consideration of multiple scattering or a treatment in the dynamical diffraction theory will be necessary even for powders.

π XAFS provides a fundamental understanding of a structure in x-ray absorption spectra far from absorption edges. A study of π XAFS in the XAFS energy range is also interesting for a detail analysis of XAFS related effects. X-ray absorption spectra measured far above and below the Pt L absorption edges showed a good agreement with the π XAFS simulation (Nishino, 2000; Tröger, 2000). Thus π XAFS can be used to study short and long range order complementary to EXAFS and diffraction techniques.

References

- Adams, B., Novikov, D. V., Hiort, T., Materlik, G. & Kossel, E. (1998). *Phys. Rev.* **B57**, 7526–7534.
- Batterman, B. W. & Cole, H. (1964). *Rev. Mod. Phys.* **36**, 681–716.
- Bedzyk, M. J. & Materlik, G. (1985). *Phys. Rev.* **B32**, 6456–6463.
- Caticha, A. & Caticha-Ellis, S. (1982). *Phys. Rev.* **B25**, 971–983.
- Gog, T., Len, P. M., Materlik, G., Bahr, D., Fadley, C. S. & Sanchez-Hanke, C. (1996). *Phys. Rev. Lett.* **76**, 3132–3135.
- Graeff, W. & Materlik, G. (1982). *Nucl. Instrum. Methods* **195**, 97–103.
- Kohra, K. & Matsushita, T. (1972). *Z. Naturforsch.* **A27**, 484–487.
- Lee, P. A. (1976). *Phys. Rev.* **B13**, 5261–5270.
- Nishino, Y. & Materlik, G. (1999). *Phys. Rev.* **B60**, 15074–15083; (2000) **B61** 14845(E).
- Nishino, Y., Tröger, L., Korecki, P. & Materlik, G. (2000) to be published.
- Ohta, T., Sekiyama, H., Kitajima, Y., Kuroda, H., Takahashi, T. & Kikuta, S. (1985). *Jpn. J. Appl. Phys.* **24**, L475–L477.
- Tröger, L., Kappen, P., Nishino, Y., Haack, N. & Materlik, G. (2000) in these proceedings.
- Zegenhagen, J. (1993). *Surf. Sci.* **18**, 199–271.